

Article

# Fuzzy Extended State Observer-Based Sliding Mode Control for an Agricultural Unmanned Helicopter

Suiyuan Shen, Jiyu Li \*, Yu Chen and Jia Lv

College of Engineering, South China Agricultural University, Guangzhou 510642, China; suiyuanshen@scau.edu.cn (S.S.); chenyu219@126.com (Y.C.); lvjia@scau.edu.cn (J.L.)

\* Correspondence: lijyu@scau.edu.cn

**Abstract:** In the context of agricultural unmanned helicopters, the complex wind disturbances over crop fields and structural perturbations due to variations in pesticide container weights present substantial challenges to flight safety. To address these issues, this paper proposes an innovative fuzzy extended state observer-based sliding mode control (FESO-SMC) methodology aimed at enhancing the aircraft's resilience against such disturbances. Initially, this study adopts a state expansion strategy to integrate both wind and structural disturbances into a comprehensive disturbance model applicable to the agricultural unmanned helicopter. Following this, a sliding mode control law is formulated with consideration for unknown total disturbances, employing specific sliding mode functions alongside exponential reaching laws. An extended state observer is simultaneously implemented within the sliding mode control framework to estimate and mitigate these disturbances, thereby augmenting the disturbance rejection capabilities of the flight control system. Additionally, the integration of fuzzy logic facilitates adaptive parameter adjustment for the extended state observer, leading to more accurate disturbance estimation. Consequently, a trajectory tracking control system tailored specifically for the agricultural unmanned helicopter has been developed, and its performance was evaluated through simulation experiments. The results indicate that, under certain disturbances, the attitude control error of the FESO-SMC controller is reduced to one-fifth that of traditional sliding mode controllers, while position control accuracy is enhanced more than twofold, thus demonstrating that the proposed FESO-SMC controller not only exhibits superior anti-disturbance capability and robustness but also achieves higher tracking accuracy compared to conventional sliding mode controller.

**Keywords:** agricultural unmanned helicopter; extended state observer; sliding mode control; fuzzy control; trajectory tracking control; anti-disturbance

Academic Editor: José Lima

Received: 2 January 2025

Revised: 20 January 2025

Accepted: 25 January 2025

Published: 30 January 2025

**Citation:** Shen, S.; Li, J.; Chen, Y.; Lv,

J. Fuzzy Extended State Observer-Based Sliding Mode Control for an Agricultural Unmanned Helicopter. *Agriculture* **2025**, *15*, 306. <https://doi.org/10.3390/agriculture15030306>

**Copyright:** © 2025 by the authors. Submitted for possible open access publication under the terms and conditions of the Creative Commons Attribution (CC BY) license (<https://creativecommons.org/licenses/by/4.0/>).

## 1. Introduction

In the realm of crop protection, chemical control remains the most effective and economically viable approach [1,2]. Compared to terrestrial spraying equipment, the agricultural unmanned helicopter exhibits distinct advantages, such as flexible take-off and landing capabilities, independence from terrain conditions, superior operational efficiency, and enhanced effectiveness [3]. Particularly, this machinery excels in managing crop diseases within challenging terrains, including mountainous and hilly areas, dense orchards, and regions where ground-based machinery faces significant limitations [4–6]. However, the operational efficacy of agricultural unmanned helicopters is often compromised by

external environmental disturbances, such as complex wind patterns and internal structural perturbations resulting from pesticide application. These disturbances can lead to flight instability, reduce the effectiveness of plant protection efforts, and pose risks to flight safety [7]. Consequently, the development of advanced flight control methodologies designed to effectively counteract these disturbances represents a critical focus area within the academic community. Such endeavors are essential for enhancing the performance and safety of agricultural unmanned helicopters, thereby ensuring their optimal utilization in crop protection.

In the field of unmanned helicopter flight control, researchers have introduced a variety of methodologies. Among these, linear control strategies such as Proportional Integral Derivative (PID) [8] and Linear Quadratic Regulator (LQR) [9] are favored for their simplicity in design and ease of engineering implementation. Despite these advantages, linear controllers are highly dependent on the precision of the flight dynamics model, which limits their effectiveness in mitigating disturbances encountered by unmanned helicopters [10]. Conversely, nonlinear control approaches provide more robust solutions to disturbance mitigation. Sliding Mode Control (SMC), characterized by its robustness, stability, rapid response, and straightforward design, has become particularly popular for unmanned helicopter flight control. For example, Ifassiouen et al. (2007) developed an SMC for a small unmanned helicopter, verifying its asymptotic stability against internal and external disturbances through Lyapunov stability analysis [11]. Similarly, Ramirez et al. (2014) presented an algorithm that combines integral sliding mode control with inversion control, ensuring sustained flight stability even under severe gust disturbances [12]. Furthermore, Derafa et al. (2012) designed a super-twisting sliding mode controller aimed at achieving precise attitude control for unmanned helicopters [13]. Liu et al. (2019) introduced an innovative exponential non-singular terminal sliding mode surface, which facilitates the online estimation and compensation of complex, unknown disturbances, thereby augmenting the robustness of unmanned aerial vehicle (UAV) attitude control. Despite this advancement, the inherent back-and-forth switching of the sliding mode controller near the sliding surface induces high-frequency chatter, posing significant risks to UAV flight safety [14]. Addressing the limitations associated with prolonged convergence times, sluggish response speeds, and substantial chattering observed in traditional sliding mode-reaching laws, Liu et al. (2017) proposed a novel fast-reaching law characterized by second-order sliding mode properties. This reaching law dynamically adjusts the approaching rate based on the distance between the current system state and the sliding mode surface, significantly enhancing the dynamic performance of the control system [15]. Although sliding mode controllers offer superior robustness against system uncertainties and disturbances compared to conventional control strategies, their design still requires certain model information about the unmanned helicopter for defining sliding mode surfaces and control laws. This prerequisite presents notable challenges in terms of obtaining accurate and comprehensive model data [16–18]. Consequently, while sliding mode control represents a significant step forward in UAV control technology, further research is needed to overcome these existing hurdles. Therefore, it is crucial to investigate alternative methodologies aimed at diminishing the reliance of sliding mode control on detailed unmanned helicopter information. Han (1991, 1994, 2009) proposed the Active Disturbance Rejection Control (ADRC) [19–21] as a viable solution, considering the characteristics of internal and external disturbances. The core principle of ADRC involves consolidating all disturbances into a total disturbance, which is then estimated using an Extended State Observer (ESO). Leveraging its real-time tracking capability, robust adaptability, and straightforward structure, ESO can effectively estimate total disturbances without necessitating the model information of the unmanned helicopter [22,23]. By substituting the component of the sliding mode control that traditionally requires model-specific

information for disturbance rejection with ESO, the flight controller achieves independence from the unmanned helicopter's model specifics. However, the adaptability of ESO must be improved, especially when confronting total disturbances exceeding predefined thresholds, which may degrade estimation performance due to suboptimal parameter settings. Fuzzy control, which translates human expertise into machine-interpretable control rules through fuzzification, offers a promising enhancement [24–26]. Researchers such as Lu (2021), Qi (2023), and Wu (2020) have successfully implemented fuzzy control strategies for online parameter tuning in ADRC controllers, achieving notable outcomes [27–29]. In this paper, we propose integrating fuzzy control mechanisms to enhance the adaptability of ESO. This integration allows for automatic adjustment of ESO parameters in response to changes in the flight status of agricultural unmanned helicopters, ensuring stable performance across varying levels of total disturbance. Consequently, this approach significantly boosts the flight controller's adaptability and anti-disturbance capabilities, thereby enhancing the operational efficiency and reliability of unmanned helicopters in agricultural applications.

In summary, this paper presents a novel control strategy based on a Fuzzy Extended State Observer-integrated Sliding Mode Control (FESO-SMC) approach. By employing an exponential reaching law to formulate the sliding mode control law, the FESO facilitates the estimation of total disturbances, enabling effective compensation within the sliding mode control framework. The proposed FESO-SMC controller is distinguished by its straightforward design and ease of implementation, rendering it exceptionally appropriate for practical deployment. Significantly, this controller exhibits robust performance in mitigating the adverse effects of complex wind disturbances and structural perturbations, thereby enhancing the overall resilience and operational efficiency of unmanned helicopters in challenging environments.

The primary objectives of this research are to eliminate internal and external disturbances affecting agricultural unmanned helicopters, thereby enhancing flight safety. This is achieved by leveraging fuzzy control to augment the ESO's disturbance observation capabilities and integrating these enhancements with the advantages of the SMC to achieve effective compensation for unknown disturbances. Consequently, this approach ensures safe and stable flight operations of agricultural unmanned helicopters. The structure of this paper is organized as follows: In the second section, we detail the design and stability analysis of a second-order FESO-SMC controller. Utilizing a six-degree-of-freedom (six-DOF) flight dynamics model specific to the agricultural unmanned helicopter, we develop a trajectory tracking control system based on the FESO-SMC controller. Subsequently, in the third section, we present simulation experiments and analyses focused on the attitude and trajectory control of the agricultural unmanned helicopter, which serve to validate the effectiveness of the proposed FESO-SMC control methodology. Finally, the fourth section concludes this paper by summarizing key findings and outcomes.

## 2. Materials and Methods

### 2.1. Second-Order Nonlinear Expansion System

Ignoring the effects of higher-order dynamics, the agricultural unmanned helicopter can be simplified into a second-order nonlinear system. Therefore, this paper expands the second-order nonlinear system and designs the corresponding fuzzy extended state observer, which can effectively estimate the disturbances faced by the agricultural unmanned helicopter.

The second-order nonlinear system under study incorporates both internal variations and external perturbations, presenting a comprehensive model for robust analysis and control synthesis:

$$\begin{cases} \dot{x}_1 = x_2 \\ \dot{x}_2 = f(x, w, t) + b(t)u \\ y = x_1 \end{cases} \quad (1)$$

where  $u$  and  $y$  represent the input and output signals, respectively. The term  $f(x, w, t)$  denotes an unknown disturbance function, whereas  $b(t)$  signifies an unknown control gain coefficient.

Define  $x_3 = f(x, w, t) + (b(t) - b_0)u$  as the newly expanded state variable, where  $x_3$  encapsulates both internal and external disturbances. Here,  $b_0$  represents a constant baseline control gain. Let the derivative of  $x_3$  with respect to time be denoted as  $\dot{x}_3 = g(t)$ . Consequently, system (1) is transformed into an extended system characterized by three state variables:

$$\begin{cases} \dot{x}_1 = x_2 \\ \dot{x}_2 = x_3 + b_0u \\ \dot{x}_3 = g(t) \\ y = x_1 \end{cases} \quad (2)$$

### 2.2. Sliding Mode Function of Second-Order Nonlinear Extended System

The error between the output of the system (2) and the target state is

$$e(t) = x_g - x_1 \quad (3)$$

$$\dot{e}(t) = \dot{x}_g - \dot{x}_1 = \dot{x}_g - x_2 \quad (4)$$

Design a sliding mode function (5)

$$s(t) = ce(t) + \dot{e}(t) \quad (5)$$

where  $x_g$  is the target state, and  $c > 0$ . When  $s(t) = 0$ , and  $ce(t) + \dot{e}(t) = 0$ , the result is  $e(t) = e(0)e^{-ct}$ . That is, when  $t \rightarrow \infty$ , the error  $e$  converges to 0 exponentially, and the convergence speed depends on the value of  $c$ . Therefore, the convergence of the sliding mode function  $s(t)$  means that the errors  $e$  and  $\dot{e}$  must be convergent. Therefore, if the control law is designed to ensure that the  $s(t)$  exponent converges to 0, the output of the second-order nonlinear system can stably track the target state.

### 2.3. Sliding Mode Control (SMC) Law

**Lemma 1 ([30]).**  $V: 0, \infty \in R$  and the solution of  $\dot{V}(t) \leq -\tau V, \forall t \geq t_0 \geq 0$  is

$$V(t) \leq e^{-\tau(t-t_0)}V(t_0) \quad (6)$$

if  $\tau$  is a positive real number, then  $V(t)$  converges exponentially to 0.

The reaching motion is expressed as the motion of the system's output, tending to the sliding mode surface  $s(t) = 0$  from any initial state. The exponential reaching law is designed as

$$\dot{s}(t) = -\varepsilon \operatorname{sgn}(s(t)) - ks(t) \quad (7)$$

where  $\varepsilon > 0, k > 0$ ; then, the output of the system can reach the sliding mode surface with good dynamic quality and can ensure rapid and stable convergence [31].

Define the Lyapunov function  $V = \frac{s^2}{2}$  combined with formula (7), then

$$\dot{V} = -\varepsilon|s| - ks^2 = -\varepsilon|s| - 2kV \leq -2kV \quad (8)$$

According to the lemma [28], the solution of Equation (8) is

$$V(t) \leq e^{-2k(t-t_0)}V(t_0) \tag{9}$$

$V(t)$  converges to 0 exponentially, and the rate of convergence of  $x$  depends on  $k$ . The exponential term  $-ks(t)$  in the exponential reaching law (7) ensures that  $s$  quickly reaches 0 from a larger initial value. The constant speed reach term  $\dot{s} = -\varepsilon \operatorname{sgn}(s(t))$  in Equation (7), ensuring that  $s$  is small and the approach velocity  $\varepsilon$  is not 0, which ensures that the system can converge in a finite time.

Derivation of Equation (5) can be obtained as follows:

$$\dot{s}(t) = c\dot{e}(t) + \ddot{e}(t) = c\dot{e}(t) + (\ddot{x}_g - \dot{x}_2) = c\dot{e}(t) + (\ddot{x}_g - x_3 - b_0u) \tag{10}$$

Combine vertical Formulas (7) and (10) to obtain Formula (11):

$$c\dot{e}(t) + (\ddot{x}_g - x_3 - b_0u) = -\varepsilon \operatorname{sgn}(s(t)) - ks(t) \tag{11}$$

Therefore, the sliding mode control law of the second-order extended system is

$$u = \frac{1}{b_0} (\varepsilon \operatorname{sgn}(s(t)) + ks(t) + \ddot{x}_g + c(\dot{x}_g - x_2) - x_3) \tag{12}$$

The total disturbance  $x_3$  is unknown, and the control law (12) is difficult to realize. Therefore, this paper adopts the FESO to estimate the state quantity  $x_1, x_2$  and total disturbance  $x_3$  of the system so as to obtain the output of the control law (12).

#### 2.4. Fuzzy Extended State Observer (FESO)

According to reference [19], the ESO of the second-order system (2) is

$$\begin{cases} e = \hat{x}_1 - y \\ \dot{\hat{x}}_1 = \hat{x}_2 - \beta_1 e \\ \dot{\hat{x}}_2 = \hat{x}_3 - \beta_2 \operatorname{fal}(e, \lambda_1, \zeta) + b_0 u \\ \dot{\hat{x}}_3 = -\beta_3 \operatorname{fal}(e, \lambda_2, \zeta) \end{cases} \tag{13}$$

$$\operatorname{fal}(e, \lambda, \zeta) = \begin{cases} \frac{e}{\zeta^{1-\lambda}}, & |e| \leq \zeta \\ |e|^\lambda \operatorname{sgn}(e), & |e| > \zeta \end{cases} \tag{14}$$

where  $\lambda_i > 0$  ( $i = 1, 2$ ),  $\beta_i > 0$  ( $i = 1, 2, 3$ ), and  $\zeta$  denotes the step size;  $\operatorname{fal}()$  represents a nonlinear function. Consequently, the output variables of the extended state observer (13) are capable of tracking the state variables and the overall disturbance of the system (2):

$$\hat{x}_1 \rightarrow x_1, \hat{x}_2 \rightarrow x_2, \hat{x}_3 \rightarrow x_3 \tag{15}$$

The gain coefficients ( $\beta_1, \beta_2$ , and  $\beta_3$ ) of the ESO are optimized within a specific operational range of the system rather than achieving global optimality. By integrating fuzzy control mechanisms into the ESO, referred to as Fuzzy ESO (FESO). The parameters  $\beta_1, \beta_2$ , and  $\beta_3$  are dynamically adjusted in real time based on varying state errors and their differential errors. This enhancement improves the adaptability and robustness of the control system.

The operational procedure is illustrated in Figure 1. Initially, the ranges of state error  $e(t)$ , differential error  $\dot{e}(t)$ , and variations  $\Delta\beta_1, \Delta\beta_2$ , and  $\Delta\beta_3$  undergo fuzzification. Subsequently, fuzzy rules are formulated to infer the fuzzy values of  $e(t)$  and  $\dot{e}(t)$  based on the fuzzy representations of  $\Delta\beta_1, \Delta\beta_2$ , and  $\Delta\beta_3$ . This process is commonly referred to as fuzzy inference. Ultimately, the defuzzification step resolves the fuzzy outputs to determine the actual values of  $\Delta\beta_1, \Delta\beta_2$ , and  $\Delta\beta_3$ .

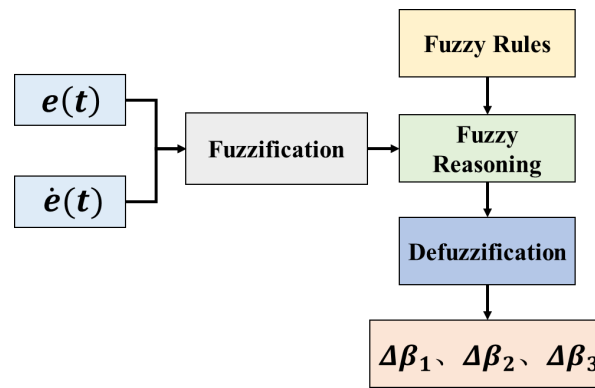


Figure 1. Adjustment algorithm of  $\beta_1, \beta_2, \beta_3$  based on fuzzy control.

The final gain coefficient of ESO is

$$\begin{cases} \beta_1(t+1) = \beta_1(t) + \Delta\beta_1(t) \\ \beta_2(t+1) = \beta_2(t) + \Delta\beta_2(t) \\ \beta_3(t+1) = \beta_3(t) + \Delta\beta_3(t) \end{cases} \quad (16)$$

### 2.4.1. Fuzzy Rules

The fuzzy controller takes  $e(t)$  and  $\dot{e}(t)$  as inputs and generates the adjustment quantities  $\Delta\beta_1, \Delta\beta_2$ , and  $\Delta\beta_3$  for  $\beta_1, \beta_2$ , and  $\beta_3$  as its outputs. Both the input and output variables of the fuzzy controller are defined across five fuzzy levels within their respective domains: {negative big (NB), negative small (NS), zero (Zo), positive small (PS), positive big (PB)}. The membership functions adopted are triangular, as depicted in Figure 2.

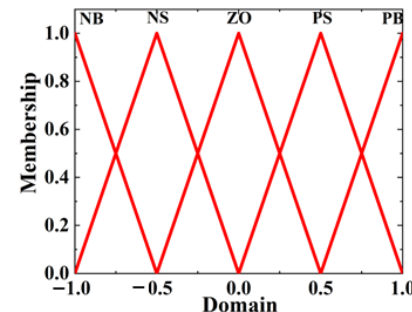


Figure 2. Triangular membership function.

### 2.4.2. Fuzzy Reasoning

Based on the parameter tuning methodology of the ESO, fuzzy rules for  $\Delta\beta_1, \Delta\beta_2$ , and  $\Delta\beta_3$  have been developed, as detailed in Tables 1, 2, and 3, respectively.

Table 1. Fuzzy rule for  $\Delta\beta_1$ .

		$\dot{e}(t)$				
		NB	NS	ZO	PS	PB
$e(t)$	NB	NB	NB	NS	NS	ZO
	NS	NS	NS	NS	ZO	ZO
	ZO	NS	ZO	ZO	ZO	PS
	PS	NS	ZO	PS	PS	PS
	PB	ZO	ZO	PS	PS	PB

**Table 2.** Fuzzy rule for  $\Delta\beta_2$ .

		$\dot{e}(t)$				
		NB	NS	ZO	PS	PB
$e(t)$	NB	NB	NS	ZO	ZO	PS
	NS	NB	NS	ZO	PS	ZO
	ZO	NS	NS	ZO	PS	PB
	PS	ZO	ZO	ZO	PS	PB
	PB	PS	PS	PS	PB	PB

**Table 3.** Fuzzy rule for  $\Delta\beta_3$ .

		$\dot{e}(t)$				
		NB	NS	ZO	PS	PB
$e(t)$	NB	NB	NB	NS	NS	ZO
	NS	NS	NS	ZO	ZO	PS
	ZO	NS	ZO	ZO	PS	PB
	PS	ZO	ZO	PS	PS	PB
	PB	PS	PS	PS	PS	PB

2.4.3. Defuzzification

The membership degrees of  $\Delta\beta_1, \Delta\beta_2$ , and  $\Delta\beta_3$  under the current input values can be determined using the established fuzzy rules. The center of gravity method is then applied to compute the precise values of  $\Delta\beta_1, \Delta\beta_2$ , and  $\Delta\beta_3$  within their respective domains.

$$\Delta\beta_j = \frac{\sum_{i=1}^N g_i S_i}{\sum_{i=1}^N S_i} \tag{17}$$

where  $S_i$  denotes the membership degree,  $g_i$  represents the fuzzy quantification value, and  $N$  indicates the fuzzy level, respectively.

The sliding mode control law (12) becomes the FESO-SMC control law based on the estimated value of unknown total disturbance  $x_3$ , that is

$$u = \frac{1}{b_0} (\varepsilon \operatorname{sgn}(s(t)) + ks(t) + \ddot{x}_g + c(\dot{x}_g - \hat{x}_2) - \hat{x}_3) \tag{18}$$

$$s(t) = c(x_g - \hat{x}_1) + (\dot{x}_g - \hat{x}_2) \tag{19}$$

FESO-SMC controller is shown in Figure 3.

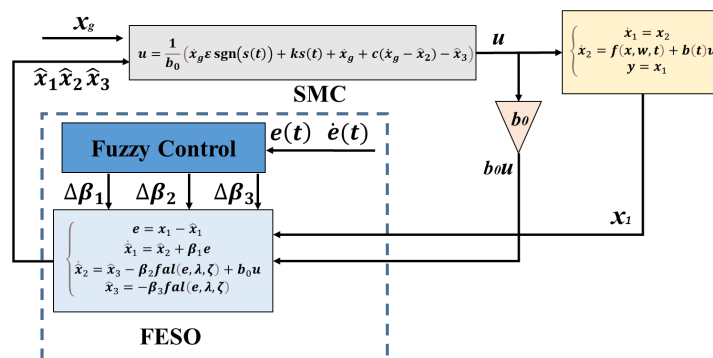


**Figure 3.** FESO-SMC controller.

2.5. Stability Analysis

Select the Lyapunov function as

$$V = \frac{s^2}{2} \tag{20}$$

And

$$\dot{V} = s\dot{s} = s(c\dot{e}(t) + \ddot{e}(t)) = s(c\dot{e}(t) + (\ddot{x}_g - \dot{x}_2)) = s(c\dot{e}(t) + (\ddot{x}_g - x_3 - b_0u)) \tag{21}$$

Substitute Equation (18) into Equation (21)

$$\dot{V} = s(-\varepsilon \operatorname{sgn} s - ks + \hat{x}_3 - x_3 + c(\hat{x}_2 - x_2)) = -\varepsilon |s| - ks^2 + s(\hat{x}_3 - x_3 + c(\hat{x}_2 - x_2)) \tag{22}$$

when the FESO is stable, the observation errors  $\hat{x}_3 - x_3, \hat{x}_2 - x_2$  tend to 0.  $\varepsilon, k$  are constants greater than 0, so  $\dot{V} \leq 0, V \geq 0$  satisfies the Lyapunov stability condition.

### 2.6. Design of the Trajectory Control System

Figure 4 depicts the architecture of the trajectory control system utilized in an agricultural unmanned helicopter [32]. The system integrates inner attitude control loops, intermediate velocity control loops, and outer position control loops, arranged hierarchically from the core to the periphery. Based on the 6-DOF flight dynamics model of the agricultural unmanned helicopter as the controlled plant, this study proposes a trajectory tracking control system founded on the FESO-SMC controller.

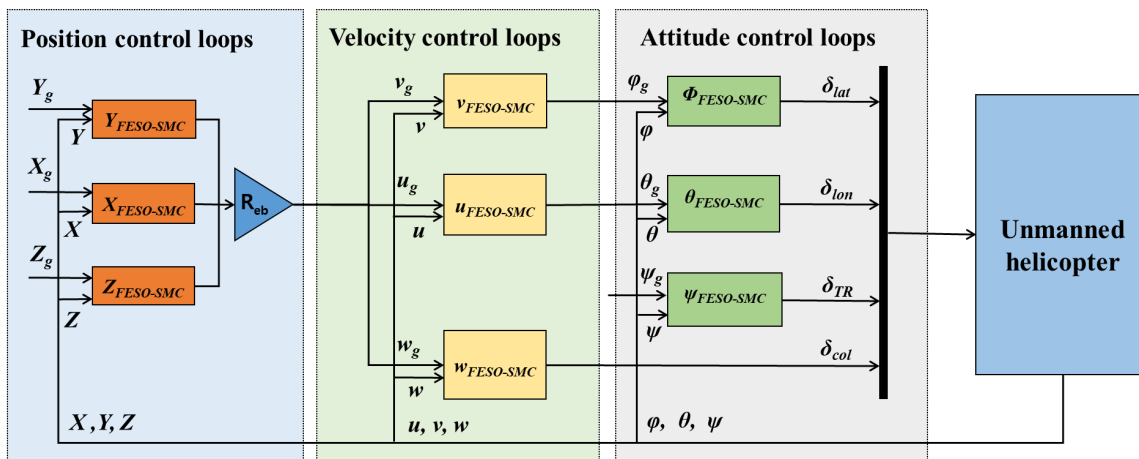


Figure 4. Trajectory control system of unmanned helicopter.

The flight dynamics equation for the 6-DOF agricultural unmanned helicopter is given by [33]:

$$\dot{\mathbf{L}} = \frac{\mathbf{F}}{m} - \boldsymbol{\Omega}\mathbf{L} \tag{23}$$

$$\dot{\mathbf{J}} = \mathbf{I}^{-1}\mathbf{M} - \mathbf{I}^{-1}\boldsymbol{\Omega}\mathbf{I} \tag{24}$$

$$\dot{\boldsymbol{\alpha}} = \mathbf{E}\mathbf{J} \tag{25}$$

$$\dot{\mathbf{P}} = \mathbf{R}_{eb}\mathbf{L} \tag{26}$$

where  $\mathbf{L} = [u \ v \ w]^T$  represents the linear velocity vector;  $\mathbf{J} = [p \ q \ r]^T$  denotes the angular velocity vector;  $\boldsymbol{\alpha} = [\phi \ \theta \ \psi]^T$  indicates the Euler angles for roll, pitch, and yaw, respectively;  $\mathbf{P} = [X \ Y \ Z]^T$  is the position vector in ground coordinates;  $m$  is the mass of the agricultural unmanned helicopter;  $\mathbf{F}$  and  $\mathbf{M}$  represent the forces and moments exerted by the components of the entire agricultural unmanned helicopter (such as the main rotor, tail rotor, fuselage, vertical stabilizer, horizontal stabilizer, etc., including gravitational forces);  $\mathbf{I}$  is the moment of inertia matrix;  $\boldsymbol{\Omega}$  is the angular rate skew-

symmetric matrix;  $\mathbf{R}_{eb}$  is the transformation matrix from body coordinates to ground coordinates, and  $\mathbf{E}$  is the transformation matrix from body angular rates to Euler angular rates, namely,

$$\mathbf{\Omega} = \begin{bmatrix} 0 & -r & q \\ r & 0 & -p \\ -q & p & 0 \end{bmatrix} \tag{27}$$

$$\mathbf{R}_{eb} = \begin{bmatrix} C_\theta C_\psi & S_\theta S_\psi C_\psi - C_\phi S_\psi & S_\theta C_\phi C_\psi + S_\phi S_\psi \\ C_\theta S_\psi & S_\theta S_\phi S_\psi + C_\phi C_\psi & S_\theta C_\phi S_\psi - S_\phi C_\psi \\ -S_\theta & S_\phi C_\theta & C_\phi C_\theta \end{bmatrix} \tag{28}$$

$$\mathbf{E} = \begin{bmatrix} 1 & S_\phi T_\theta & T_\theta C_\phi \\ 0 & C_\phi & -S_\phi \\ 0 & S_\phi / C_\theta & C_\phi / C_\theta \end{bmatrix} \tag{29}$$

Treat Equations (24) and (25) as

$$\dot{\boldsymbol{\alpha}} = \mathbf{F}_1(\boldsymbol{\alpha})\mathbf{J} \tag{30}$$

$$\dot{\mathbf{J}} = \mathbf{F}_2(\boldsymbol{\alpha}, \mathbf{J}, \mathbf{L}, \boldsymbol{\Omega}, \mathbf{w}) + \mathbf{B}(\boldsymbol{\alpha}, \mathbf{J}, \mathbf{L}, \boldsymbol{\Omega}, \mathbf{w})\mathbf{U}_c \tag{31}$$

where  $\mathbf{w}$  represents the disturbance, and  $\mathbf{U}_c = [\delta_{lon} \quad \delta_{lat} \quad \delta_{TR}]$  is the control vector consisting of the longitudinal pitch, lateral pitch, and tail rotor pitch. By combining Equations (30) and (31), a second-order system of state equations can be derived as follows:

$$\ddot{\boldsymbol{\alpha}} = \frac{d\mathbf{F}_1}{dt}\mathbf{J} + \mathbf{J}\mathbf{F}_1 = \mathbf{F}_3\mathbf{S} + \mathbf{F}_1(\mathbf{F}_2 + \mathbf{B}\mathbf{U}_c) \tag{32}$$

where,  $\mathbf{F}_3 = d\mathbf{F}_1 / dt$ ,  $\mathbf{F}_1, \mathbf{F}_2$ , and  $\mathbf{B}$  are the corresponding matrices or abbreviations. The total disturbance is expressed as  $\bar{\mathbf{f}}_\alpha = \mathbf{F}_3\mathbf{S} + \mathbf{F}_1(\mathbf{F}_2 + \mathbf{B}\mathbf{U}_c) - \mathbf{B}_{0\alpha}\mathbf{U}_c$ . Substituting this expression into Equation (32), the equation is transformed into a second-order nonlinear system:

$$\ddot{\boldsymbol{\alpha}} = \bar{\mathbf{f}}_\alpha + \mathbf{B}_{0\alpha}\mathbf{U}_c \tag{33}$$

where  $\mathbf{B}_{0\alpha}$  is the gain matrix for attitude control. The control vector  $\mathbf{U}_c$ , comprising the pitch, roll, and yaw loop control variables, along with the output  $\boldsymbol{\alpha}$ , establishes a single-input–single-output (SISO) relationship.

Define  $\mathbf{x}_1 = \boldsymbol{\alpha}$ ,  $\mathbf{x}_2 = \dot{\boldsymbol{\alpha}}$ ,  $\mathbf{x}_3 = \bar{\mathbf{f}}_\alpha$ ,  $\dot{\mathbf{x}}_3 = \mathbf{g}(t)$ . The original system is then expanded to form an integrated second-order system, denoted as System (34), analogous to the expanded system described in Equation (2).

$$\begin{cases} \dot{\mathbf{x}}_1 = \mathbf{x}_2 \\ \dot{\mathbf{x}}_2 = \mathbf{x}_3 + \mathbf{B}_{0\alpha}\mathbf{U}_c \\ \dot{\mathbf{x}}_3 = \mathbf{g}(t) \\ \mathbf{y} = \mathbf{x}_1 \end{cases} \tag{34}$$

Therefore, the pitch, roll, and yaw attitude control loops can each be designed using a second-order FESO-SMC control structure. The velocity control loop provides commands for the pitch angle and roll angle, while the yaw angle commands are directly derived from the mission command. The output of the attitude control loop is the control vector  $[\delta_{lon} \quad \delta_{lat} \quad \delta_{TR}]$ , which includes the longitudinal, lateral, and tail rotor pitch commands.

Based on the foregoing analysis, the longitudinal pitch control  $\delta_{lon}$  is designed as follows:

$$\begin{cases} e = \hat{x}_1 - \theta \\ \dot{\hat{x}}_1 = \hat{x}_2 - \beta_1(t+1)e \\ \dot{\hat{x}}_2 = \hat{x}_3 - \beta_2(t+1)fal(e, \lambda, \zeta) + b_{0\theta}u \\ \dot{\hat{x}}_3 = -\beta_3(t+1)fal(e, \lambda_2, \zeta) \\ \beta_1(t+1) = \beta_1(t) + \Delta\beta_1(t) \\ \beta_2(t+1) = \beta_2(t) + \Delta\beta_2(t) \\ \beta_3(t+1) = \beta_3(t) + \Delta\beta_3(t) \\ s(t) = c(\theta_g - \hat{x}_1) + (\dot{\theta}_g - \hat{x}_2) \\ \delta_{lon} = \frac{1}{b_{0\theta}}(\varepsilon \operatorname{sgn}(s(t)) + ks(t) + \ddot{\theta}_g + c(\dot{\theta}_g - \hat{x}_2) - \hat{x}_3) \end{cases} \quad (35)$$

where  $\theta_g$  is the output signal from the longitudinal velocity loop;  $\theta$  is the pitch angle signal of the agricultural unmanned helicopter;  $b_{0\theta}$  denotes the control gain, and  $\hat{x}_1, \hat{x}_2$  are the estimated value and its derivative of  $\theta$ ,  $\hat{x}_3$  is the estimated total disturbance of the attitude loop.

The design of the roll loop control  $\delta_{lat}$  and the yaw loop control  $\delta_{TR}$  follows a similar approach and will not be reiterated here. The calculation methods for the velocity and position control loops are analogous to Equation (35), with the differences lying in the physical meanings and symbols of the variables involved.

### 3. Results and Discussion

#### 3.1. Simulation Results of Attitude Control

The simulation experiment was executed using the Matlab/Simulink 2022b numerical simulation software. The experimental configuration is detailed as follows: the agricultural unmanned helicopter’s initial attitude is set to  $0^\circ$ , with a target attitude of  $5^\circ$ . The chosen agricultural unmanned helicopter model is the ALIGN E1 PLUS, as illustrated in Figure 5, with its initial parameter values delineated in Table 4. The simulation experiment utilizes both the SMC designed in [31] and the FESO-SMC controller developed in this study. Table 5 presents the parameters for both the SMC controller and the FESO-SMC controller.

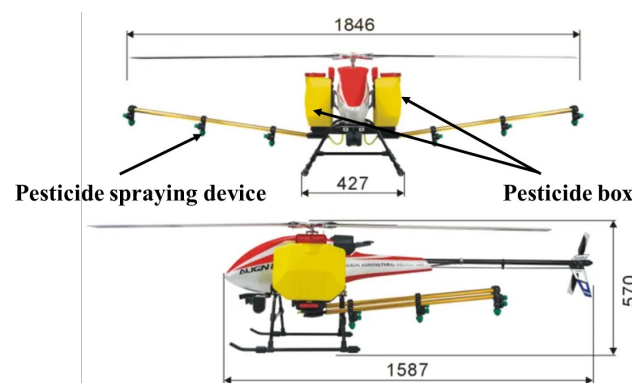


Figure 5. The agricultural unmanned helicopter (ALIGN E1 PLUS).

Table 4. Main parameters of the ALIGN E1 PLUS.

Parameter	Unit	Initial Value	Modify Value
Mass	kg	30	15
Rotor radius	m	0.923	0.923
Tail rotor radius	m	0.157	0.157

Rotor speed	rad/s	195	195
Tail rotor speed	rad/s	1146	1146
Inertia coefficient $I_x$	kg · m <sup>2</sup>	0.51	0.42
Inertia coefficient $I_y$	kg · m <sup>2</sup>	0.69	0.57
Inertia coefficient $I_z$	kg · m <sup>2</sup>	1.26	0.91

**Table 5.** Parameters of attitude controllers.

$[\phi \ \theta \ \psi]$	SMC	FESO-SMC
c	[92 114 105]	[108 129 95]
$\varepsilon$	[0.52 2.15 0.55]	[0.65 2.74 0.45]
k	[187 126 209]	[268 96 175]
$b_0$	[1.54 0.39 0.65]	[1.65 0.52 0.69]
dL	[-50 -20 -20]	-
dU	[20 20 50]	-
$\beta_1$	-	[79 49 127]
$\beta_2$	-	[470 71 190]
$\beta_3$	-	[52 41 55]
$\xi$	-	[0.005 0.01 0.01]

### 3.1.1. Anti-Disturbance Test

External wind disturbances represent a critical challenge to the stable flight operations of agricultural unmanned helicopters. To simulate sudden wind disturbances, a rectangular wave signal is introduced within a specified timeframe. The initial parameters for the agricultural unmanned helicopter are configured according to those detailed in Table 4. At the fifth second of the simulation, a rectangular wave disturbance with an amplitude of 10 and a pulse width of 1 s is applied to the model of the agricultural unmanned helicopter, as depicted in Figure 6. Under normal operating conditions without external disturbances, both the SMC and the FESO-SMC exhibit similar levels of control effectiveness, enabling the agricultural unmanned helicopter to rapidly stabilize to the desired target attitude angle. However, upon introducing the rectangular wave signal at the fifth second, a notable divergence in performance is observed: the FESO-SMC controller maintains stability in attitude, whereas the SMC controller shows significant fluctuations. This indicates that the FESO-SMC controller is more effective in ensuring stability under sudden disturbance conditions, thereby demonstrating its superior capability in mitigating the adverse effects of external disturbances on flight stability. The SMC controller has a maximum fluctuation of no more than  $0.1^\circ$ , and the FESO-SMC has a maximum fluctuation of no more than  $0.02^\circ$ , which is only one-fifth of the SMC controller. Figure 7 illustrates the estimated response curve of the FESO relative to the flight state and total disturbance. Initially, the FESO demonstrates a significant output in attitude rate, approaching approximately 700, which facilitates swift tracking of the target attitude. As the system approaches convergence with the target attitude, the estimation error of the FESO for both attitude and attitude rate markedly decreases, nearing zero. This reduction underscores the robustness and precision of the FESO's estimation capabilities concerning the flight state. In the absence of external disturbances, the FESO effectively tracks gradual changes in the estimated total disturbance. Upon the introduction of an external disturbance at the fifth second, characterized by a sudden increase of about 20 units in one second in the variable  $x_3$ , the FESO promptly detects this variation in total disturbance. This rapid detection significantly enhances the anti-disturbance capability of the FESO-Sliding Mode Control (FESO-SMC) controller, thereby reinforcing its effectiveness in maintaining stability and control accuracy under disturbed conditions.

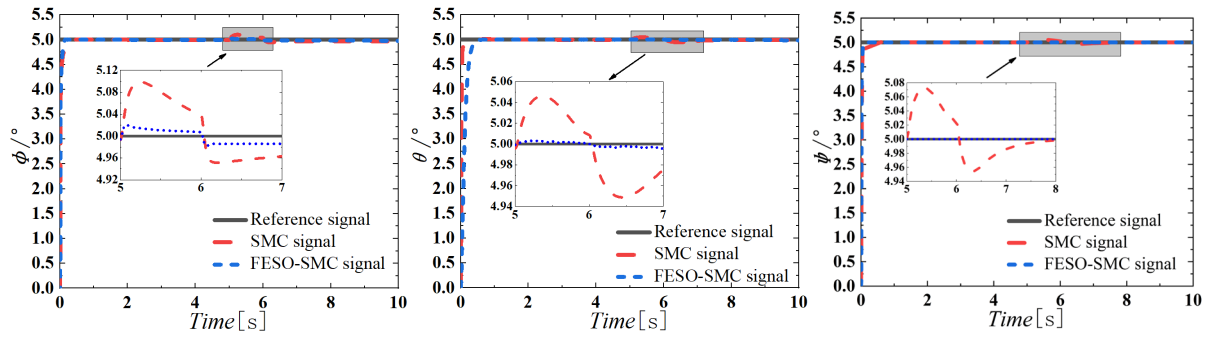


Figure 6. Response curve of anti-disturbance test.

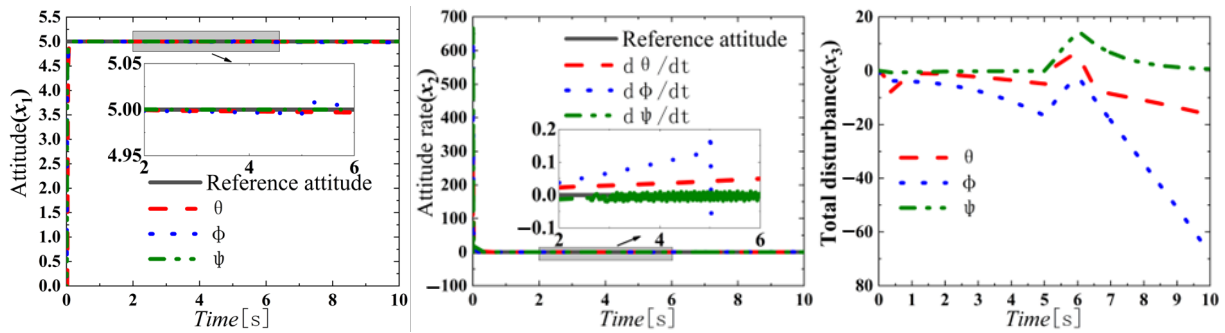
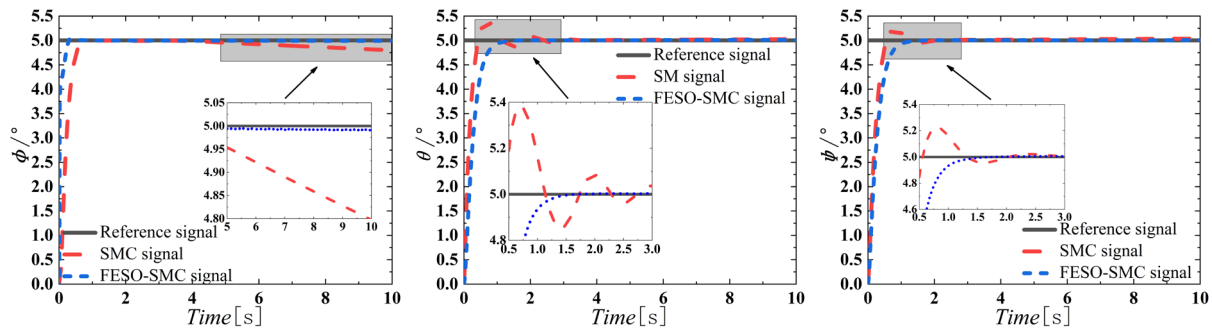


Figure 7. Estimation curve of FESO for flight state  $(x_1, x_2)$  and total disturbance  $x_3$ .

### 3.1.2. Robustness Test

As large quantities of pesticides are dispensed over farmland, the weight and inertia of the agricultural unmanned helicopter undergo significant reductions, potentially impacting the flight controller’s adaptation to the altered structural characteristics. This can lead to a degradation in flight control performance. Such changes in the agricultural unmanned helicopter’s structural parameters—representing internal disturbances—are characterized by a halving of the weight reduction and approximately a 20% decrease in inertia, as detailed in Table 4, while the controller parameters remain unchanged. Figure 8 presents the simulation outcomes under these conditions. Despite substantial alterations in the structural parameters of the agricultural unmanned helicopter, the FESO-SMC demonstrates consistently superior dynamic response compared to the traditional SMC. Specifically, from the fifth second onwards, the roll angle controlled by the SMC decreases gradually by  $0.2^\circ$  over five seconds, whereas the FESO-SMC maintains a stable roll angle. Additionally, the pitch angle under SMC fluctuates by nearly  $0.4^\circ$ , while the FESO-SMC shows neither overshoot nor fluctuation. Similarly, the yaw angle under SMC exhibits fluctuations of up to  $0.2^\circ$ , whereas the FESO-SMC continues to display no signs of overshoot or fluctuation. These simulation results substantiate that the FESO-SMC controller not only possesses robustness but also effectively mitigates disturbances arising from structural changes within the agricultural unmanned helicopter, thereby ensuring enhanced stability and control accuracy.



**Figure 8.** Response curve of robustness test.

### 3.2. Simulation Results of Trajectory Control

The ‘8’-figure climbing maneuver is selected as the benchmark flight task for evaluating the performance of both the SMC as described in [31] and the newly introduced FESO-SMC discussed herein. The initial parameters of the agricultural unmanned helicopter are provided in Table 4, while the specific control parameters for both the SMC and FESO-SMC are detailed in Table 6. At the 5 s mark of the simulation, a rectangular wave disturbance with an amplitude of 10 and a pulse width of 10 s is introduced into the attitude control loop to simulate external disturbances. Additionally, at the 20 s mark, the structural parameters of the agricultural unmanned helicopter are adjusted according to the modified values specified in Table 4, which include a significant reduction in weight and a corresponding decrease in inertia. It is important to note that during this adjustment, the controller parameters remain unchanged to evaluate the controllers’ robustness against such internal perturbations. This methodology allows for a comprehensive assessment of the stability and effectiveness of both control strategies under varying conditions.

The simulation outcomes are illustrated in Figures 9–11. Upon the introduction of a rectangular wave disturbance, the trajectory controlled by the SMC exhibits significant fluctuations, leading to a considerable increase in tracking error. Specifically, the maximum error reached over 6 m in the X direction and exceeded 12 m in the Y direction. In contrast, the FESO-SMC maintains high-precision trajectory tracking with errors confined within 2 m. Even after the disturbance has subsided, the SMC controller’s tracking error does not diminish promptly, resulting in a notable deviation from the desired trajectory. Conversely, the FESO-SMC controller effectively and swiftly estimates the total disturbances encountered by the agricultural unmanned helicopter—evident from the significant variations in the estimates of  $x_3$  during perturbations—and provides feedback to the SMC control law for precise compensation. Consequently, the FESO-SMC controller achieves trajectory tracking that is closely aligned with the predetermined path. Upon altering the structural parameters of the agricultural unmanned helicopter, the performance discrepancy becomes even more pronounced. The SMC controller exhibits sustained position fluctuations of up to 4 m, whereas the FESO-SMC controller demonstrates minimal deviation. These simulation results highlight the superior anti-disturbance capabilities and robustness of the FESO-SMC controller, ensuring high-accuracy trajectory tracking for agricultural unmanned helicopters under varying conditions. This enhanced performance validates the effectiveness of integrating FESO with SMC in improving the operational reliability and precision of unmanned aerial systems.

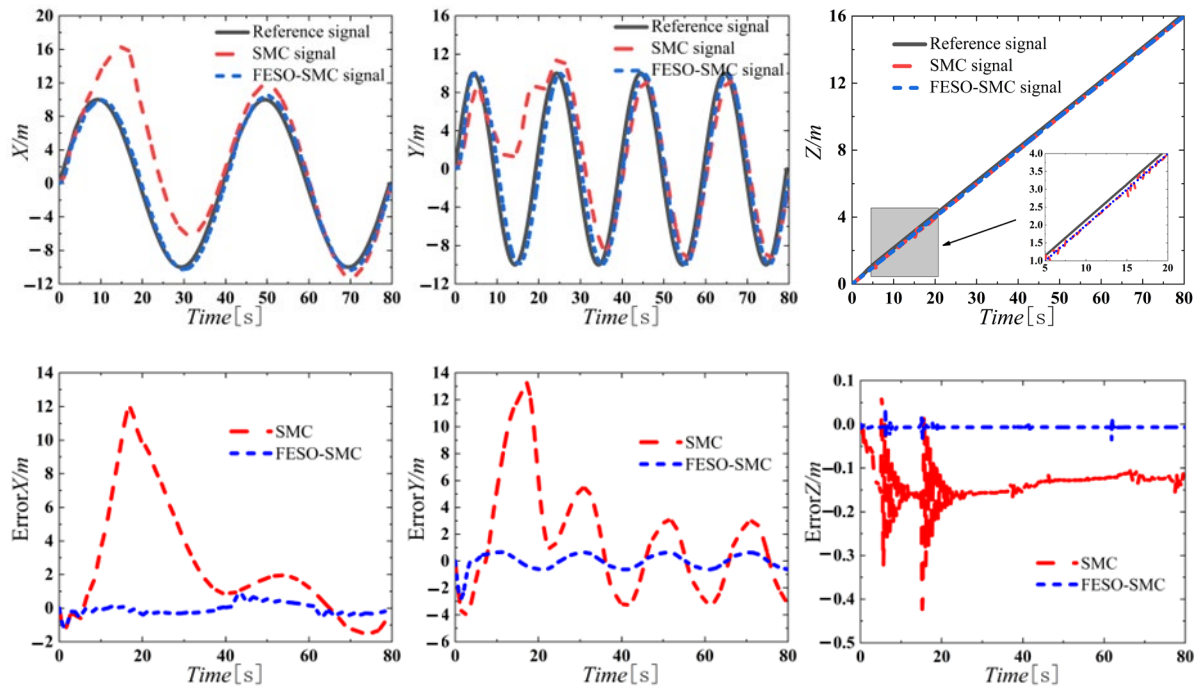


Figure 9. Trajectory tracking response in X, Y, Z.

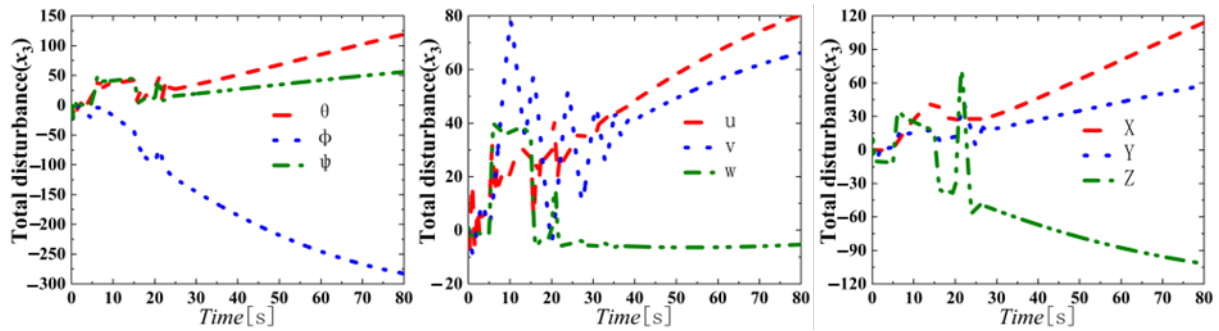


Figure 10. Estimation curve of FESO for total disturbance  $x_3$ .

Table 6. Parameters of controllers.

	Attitude (SMC)	Attitude (FESO-SMC)	Velocity (SMC)	Velocity (FESO-SMC)	Position (SMC)	Position (FESO-SMC)
c	[67 81 77]	[52 78 65]	[52 57 72]	[45 46 95]	[99 121 110]	[87 85 91]
$\varepsilon$	[0.45 1.56 0.58]	[0.35 1.24 0.71]	[1.42 0.79 0.55]	[1.15 1.12 0.52]	[0.77 4.35 1.28]	[1.25 5.01 2.32]
k	[156 150 170]	[124 128 165]	[121 136 52]	[101 105 56]	[57 60 98]	[41 65 86]
$b_0$	[1.55 0.41 0.58]	[1.15 0.32 0.65]	[7.22 9.45 1.24]	[7.21 9.35 1.27]	[1.25 0.84 0.87]	[2.41 0.79 0.92]
dL	[-50 -20 -20]	-	[-10 -20 -70]	-	[-60 -50 -40]	-
dU	[20 20 50]	-	[80 50 50]	-	[180 20 100]	-
$\beta_1$	-	[74 65 145]	-	[412 105 27]	-	[30 45 96]
$\beta_2$	-	[505 61 208]	-	[124 112 53]	-	[212 79 180]
$\beta_3$	-	[64 32 51]	-	[42 45 72]	-	[101 97 82]
$\xi$	-	[0.005 0.01 0.01]	-	[0.01 0.01 0.01]	-	[0.01 0.01 0.01]

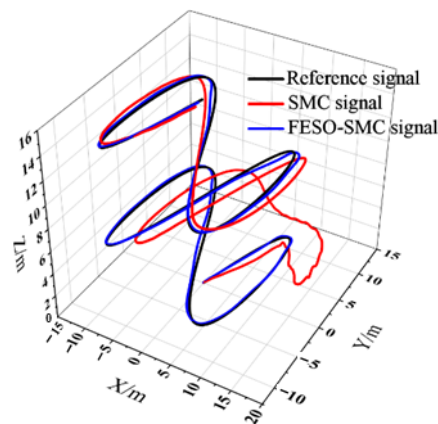


Figure 11. Trajectory tracking response.

#### 4. Conclusions

This paper introduces a design methodology for a SMC that incorporates a FESO. Initially, the system is reformulated into a standard series system that includes terms for total disturbances. Subsequently, the FESO is employed to estimate these unknown total disturbance terms, which are then compensated within the sliding mode control law to derive the controller's output. The proposed FESO-SMC controller effectively mitigates the impacts of both internal and external disturbances, thereby achieving precise control over the position and attitude of agricultural unmanned helicopters. This approach not only enhances the robustness of the control system but also ensures reliable performance under varying operational conditions, making it highly suitable for practical applications in agriculture. Simulation verification fully shows the following:

- (1) The FESO exhibits robust adaptive capabilities, effectively managing significant disturbances. Upon a change in disturbance, the FESO rapidly estimates and compensates for this variation within a single second, ensuring prompt disturbance rejection;
- (2) The FESO-SMC controller proposed in this study maintains attitude stability and achieves high-precision trajectory tracking for agricultural unmanned helicopters. Notably, even under conditions of strong wind disturbances and structural perturbations, the FESO-SMC controller sustains high-precision tracking control. Specifically, the attitude control error of the FESO-SMC controller is merely one-fifth that of the traditional SMC controller, while its position control accuracy exceeds twice that of the SMC controller when subjected to disturbances. These findings highlight the superior anti-disturbance capabilities and enhanced robustness of the FESO-SMC controller compared to conventional SMC methods, underscoring its effectiveness in improving the operational reliability and precision of agricultural unmanned helicopters.

**Author Contributions:** Conceptualization, S.S. and J.L. (Jiyu Li); methodology, S.S.; software, Y.C.; validation, S.S.; formal analysis, S.S.; investigation, S.S.; resources, J.L. (Jiyu Li) and J.L. (Jia Lv); data curation, S.S.; writing—original draft preparation, S.S.; writing—review and editing, J.L. (Jiyu Li); visualization, Y.C.; supervision, S.S.; project administration, J.L. (Jiyu Li); funding acquisition, S.S. All authors have read and agreed to the published version of the manuscript.

**Funding:** This research was funded by the National Natural Science Foundation of China (62403203), the Science and Technology Projects in Guangzhou (2025A04J4161), and the Specific University Discipline Construction Project (2023B10564002).

**Institutional Review Board Statement:** Not applicable.

**Data Availability Statement:** Data are contained within the article.

**Conflicts of Interest:** The authors declare no conflicts of interest.

## References

1. Zhao, D.; Simon, C.; Parmjit, C. Development and characterization of a contact-charging electrostatic spray UAV system. *Agriculture* **2024**, *14*, 467.
2. Fuentealba, A.; Dupont, A.; Hébert, C.; Berthiaume, R.; Quezada-García, R.; Bauce, É. Comparing the efficacy of various aerial spraying scenarios using *Bacillus thuringiensis* to protect trees from spruce budworm defoliation. *For. Ecol. Manag.* **2019**, *432*, 1013–1021.
3. Zhang, H.; Wang, L.; Tian, T.; Yin, J. A review of unmanned aerial vehicle low-altitude remote sensing (UAV-LARS) use in agricultural monitoring in China. *Remote Sens.* **2021**, *13*, 1221.
4. Fan, B.; Li, Y.; Zhang, R.; Fu, Q. Review on the technological development and application of UAV systems. *Chin. J. Electron.* **2020**, *29*, 199–207.
5. Radoglou-Grammatikis, P.; Sarigiannidis, P.; Lagkas, T.; Moscholios, I. A compilation of UAV applications for precision agriculture. *Comput. Netw.* **2020**, *172*, 107148.
6. Aleksandra, P.; Bogusława, B.; Jerzy, C. Propellers spin rate effect of a spraying drone on quality of liquid deposition in a crown of young spruce. *Agriculture* **2023**, *13*, 1584.
7. Martins, L.; Carlos, C.; Oliveira, P. Inner-outer feedback linearization for quadrotor control: Two-step design and validation. *Nonlinear Dyn.* **2022**, *110*, 479–495.
8. Zhang, X.; Xian, B.; Zhao, B. Autonomous flight control of a nano quadrotor helicopter in a GPS-denied environment using on-board vision. *IEEE Trans. Ind. Electron.* **2015**, *62*, 6392–6403.
9. Case, C.; Suresh, B.; Coates, A. Autonomous sign reading for semantic mapping. In Proceedings of the IEEE International Conference on Robotics and Automation, Shanghai, China, 9–13 May 2011.
10. Ghadiri, H.; Emam, M.; Khodadadi, H. Adaptive super-twisting non-singular terminal sliding mode control for tracking of quadrotor with bounded disturbances. *Aerosp. Sci. Technol.* **2021**, *112*, 106616.
11. Ifassiouen, H.; Guisser, M.; Medromi, H. Robust nonlinear control of a miniature autonomous helicopter using sliding mode control structure. *Int. J. Mech. Aerosp. Ind. Mechatron. Eng.* **2007**, *1*, 84–89.
12. Ramirez-Rodriguez, H.; Parra-Vega, V.; Sanchez-Orta, A. Robust backstepping control based on integral sliding modes for tracking of quadrotors. *J. Intell. Robot. Syst.* **2014**, *73*, 51–66.
13. Derafa, L.; Benallegue, A.; Fridman, L. Super twisting control algorithm for the attitude tracking of a four rotors UAV. *J. Frankl. Inst.-Eng. Appl. Math.* **2012**, *349*, 685–699.
14. Liu, B.; Wang, P.; Sha, L. Attitude control for QTR using exponential nonsingular terminal sliding mode control. *J. Syst. Eng. Electron.* **2019**, *30*, 191–200.
15. Liu, H.; Wang, H.; Shen, L. Attitude control for vertical take off and landing mode of QTR based on fractional order sliding mode control. *Syst. Eng. Electron.* **2017**, *39*, 156–161.
16. Maqsood, H.; Qu, Y. Nonlinear disturbance observer based sliding mode control of quadrotor helicopter. *J. Electr. Eng. Technol.* **2020**, *15*, 1453–1461.
17. Chen, Y.; Wu, S.; Wang, X. Time and FOV constraint guidance applicable to maneuvering target via sliding mode control. *Aerosp. Sci. Technol.* **2023**, *133*, 108104.
18. Zhang, N.; Qi, W.; Park, J.H. Sliding mode control for discrete-time singular semi-Markovian jumping models. *Inf. Sci.* **2023**, *624*, 554–566.
19. Han, J. State feedback realization of nonlinear control systems. *Control Decis.* **1991**, *21*, 161–167.
20. Han, J. A new type of controller: NLPID. *Control Decis.* **1994**, *24*, 401–407.
21. Han, J. From PID to active disturbances rejection control. *IEEE Trans. Ind. Electron.* **2009**, *56*, 900–906.
22. Guo, B.; Wu, Z.; Zhou, H. Active disturbance rejection control approach to output-feedback stabilization of a class of uncertain nonlinear systems subject to stochastic disturbance. *IEEE Trans. Autom. Control* **2016**, *61*, 1613–1618.
23. Shen, S.; Xu, J. Trajectory tracking active disturbance rejection control of the unmanned helicopter and its parameters tuning. *IEEE Access* **2021**, *9*, 56773–56785.
24. Zhang, J.; Yang, G. Low-computation adaptive fuzzy tracking control of unknown nonlinear systems with unmatched disturbances. *IEEE Trans. Fuzzy Syst.* **2020**, *28*, 321–332.
25. Navabi, M.; Hashkavaei, N.S.; Reyhanoglu, M. Satellite attitude control using optimal adaptive and fuzzy controllers. *Acta Astronaut.* **2023**, *204*, 434–442.

26. Cui, D.; Xiang, Z. Nonsingular fixed-time fault-tolerant fuzzy control for switched uncertain nonlinear systems. *IEEE Trans. Fuzzy Syst.* **2023**, *31*, 174–183.
27. Lu, W.; Li, Q.; Lu, K. Load adaptive PMSM drive system based on an improved ADRC for manipulator joint. *IEEE Access* **2021**, *9*, 33369–33384.
28. Qi, B.; Wang, P.; Chai, X. Mirror milling trajectory planning for large thin-walled parts based on Fuzzy-ADRC controlled force pre-supporting. *J. Manuf. Process.* **2023**, *85*, 192–204.
29. Wu, Y.; Chen, Z.; Su, L. Longitudinal attitude control of quad tilt-rotor UAV based on fuzzy LADRC. *Flight Dyn.* **2020**, *38*, 28–33.
30. Ioannou, P.A.; Sun, J. *Robust Adaptive Control*; Prentice-Hall: Englewood Cliffs, NJ, USA, 1996; p. 274.
31. Liu, J. *Sliding Mode Control Design and MATLAB Simulation*, 3rd ed.; Tsinghua University Press: Beijing, China, 2015; p. 46.
32. Shen, S.; Xu, J. Adaptive neural network-based active disturbance rejection flight control of an unmanned helicopter. *Aerosp. Sci. Technol.* **2021**, *119*, 107062.
33. Wu, C.; Wang, H.; Zhang, Y. Trajectory tracking of Unmanned Helicopter based on LADRC. *Acta Aeronaut. Sin.* **2015**, *36*, 473–483.

**Disclaimer/Publisher's Note:** The statements, opinions and data contained in all publications are solely those of the individual author(s) and contributor(s) and not of MDPI and/or the editor(s). MDPI and/or the editor(s) disclaim responsibility for any injury to people or property resulting from any ideas, methods, instructions or products referred to in the content.